DAPNIA-STCM-98-12

CEA/SACLAY
DSM

SERVICE TECHNIQUE DE CRYOGÉNIE ET DE MAGNÉTISME

OCT 21 1998
LIBRARY

Fermilab Library
0 1160 0067861 9

I.D No. M.S.

DAPNIA/STCM 98-12 September 1998

INTERSTRAND RESISTANCE MEASUREMENTS ON Nb_3Sn RUTHERFORD-TYPE CABLES

A. Devred, L. Bacquart, P. Bredy, C.E. Bruzek, Y. Laumond, R. Otmani, T. Schild

DAPNIA

Paper presented at the Applied Superconductivity Conference (ASC'98), Palm Desert, California (U.S.A.), September 13-18, 1998

Département d'**A**strophysique, de Physique des **P**articules, de Physique **N**ucléaire et de l'**I**nstrumentation **A**ssociée
CEA/Saclay F-91191 Gif-sur-Yvette Cédex

Couverture : Sylvie Cabrit et Marc Sauvage

Interstrand Resistance Measurements on Nb_3Sn Rutherford-Type Cables

A. Devred,[1] L. Bacquart,[1] P. Bredy,[1] C.E. Bruzek,[2] Y. Laumond,[2] R. Otmani,[1] and T. Schild[3]

[1]CEA/Saclay, DSM/DAPNIA/STCM, F–91191 Gif-Sur-Yvette Cedex, FRANCE
[2]Alstom, EMG/MSA/Fil, 3bis avenue des Trois Chênes, F–90018 Belfort Cedex, FRANCE
[3]CEA/Cadarache, DSM/DRFC/STID, F–13108 Saint-Paul-les-Durance Cedex, FRANCE

***Abstract*—We review a series of interstrand resistance measurements performed on two Rutherford-type cables made from unplated niobium-tin strands produced by Alstom: a regular cable and a cable with a stainless steel core inserted between the two strand layers. The interstrand resistance measurements are interpreted in terms of crossover and adjacent resistances and are compared to published data on similar cables.**

I. Introduction

Accelerator magnet coils are wound from flat, two-layer, Rutherford-type cables made up of a few tens of strands twisted together [1]. Such geometry presents two types of interstrand contacts: (1) discrete contacts at the crossovers between strands of the two layers and (2) continuous contacts between adjacent strands of a same layer. The strand deformations due to cabling and the high pre-compressions applied to the coil during magnet assembly can result in low contact resistances. When the cable is subjected to a transverse, time-varying field, the network of interstrand resistances is the seat of current loops, which distort field quality [2], [3]. The field distortions are very damageable for accelerator operation, even for a slow-ramping machine, such as the Large Hadron Collider (LHC). (The LHC ramp rate is 10 A/s, which, for its dipole magnets, corresponds to a field ramp rate of about 7.5 mT/s.)

The effects of interstrand coupling currents can be limited by developing large interstrand resistances. However, it is also desirable to keep the strands from being electrically insulated from each other, to preserve the possibility of interstrand current redistribution [4], [5]. A compromise must be found between these conflicting demands, and the cables must be designed and manufactured so as to ensure a suitable, reproducible and uniform level of interstrand resistances in the magnet coil assemblies. For LHC cables, the target value of crossover resistance is 20 μΩ ± 10 μΩ.

The interstrand resistances have several components which are detailed elsewhere [6]. Among them, are the resistances of the metallic rings surrounding the multifilamentary areas within the cable strands, and the resistances of the oxide layers that develop on the strand surfaces. For regular cables, this last component is usually the most determinant and the most difficult to control. Attempts have also been made to increase crossover resistances by inserting a thin, insulating core between the two layers of strands [7].

In this paper, we compare the results of interstrand resistance measurements performed on a regular and on a cored Rutherford-type cable made from the same unplated Nb_3Sn strands. Strands and cables were produced by Alstom.

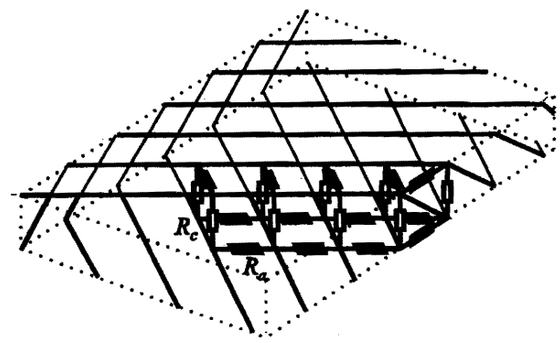

Fig. 1. Rutherford-Type Cable Model [10].

II. Cable Model

Fig. 1 presents the equivalent electrical circuit used to represent an N-strand Rutherford-type cable in the steady state or subjected to a magnetic field varying at a constant rate. This circuit was first developed for a braided conductor [8] and was later extended to Rutherford-type conductors [9]–[11].

In the model of Fig. 1, the strands are represented by equipotential lines. Over a twist pitch, each strand crosses two times every other strand. The crossings are represented by elementary resistances, referred to as *crossover resistances*, R_c. The points where the crossover resistances are connected to the lines define the network nodes. Furthermore, the continuous contacts between adjacent strands are represented by discrete elementary resistances, referred to as *adjacent resistances*, R_a, connected to the network nodes. Over a pitch length, each strand encounters $(2N–2)$ crossover resistances and is connected to each of its neighbors by $(2N)$ adjacent resistances. In the following, R_a and R_c are assumed to be uniform.

When subjecting the cable of Fig. 1 to an uniform, transverse field, B_t, varying at a constant rate, the power per unit volume, P_c, dissipated in the crossover resistances is [2]

$$P_c \approx \frac{N^2 w L_p}{120 h R_c}\left(\frac{dB_t}{dt}\right)^2 \tag{1}$$

where w is the cable width, h is the average cable thickness and L_p is the cable pitch length.

Similarly, the power per unit volume, P_a, dissipated by the coupling currents in the adjacent resistances is [9]

$$P_a \approx \frac{w L_p}{6 h R_a}\left(\frac{dB_t}{dt}\right)^2 \tag{2}$$

Equations (1) and (2) show that, to obtain similar levels of power dissipation, R_a and R_c should be in the ratio $(20/N^2)$. For our cables, $N = 36$, which implies that R_a must be about 65 times smaller than R_c. The interstrand coupling currents of regular cables are usually dominated by crossover resistances, while adjacent resistances dominate those of cored cables [7], [12].

III. SAMPLE PREPARATION

Two different cables were investigated: (1) a cable made from unplated Nb_3Sn strands, referred to as ALS1 and (2) a cable made from the same strands but with a 13 mm x 0.025 mm stainless steel (316L) core, referred to as ALS2.

The strands were manufactured according to the internal-tin process [13]. Their diameter is 0.78 mm. They are made up of seven subelements surrounded by two barriers (an inner one in tantalum and an outer one in niobium) and a copper outer sheath. The copper-to-non-copper ratio is 1.2 to 1. The sub-elements include 408 niobium–7.5wt% tantalum filaments arranged in three concentric circles in a copper matrix around a tin pool. The Nb_3Sn compound formation requires a heat treatment, during which tin diffuses through the copper matrix and reacts with the Nb filaments. The barriers prevent tin pollution in the Cu outer sheath and preserve its resistivity.

The two cables have the same parameters: 36 strands, a pitch length of 73 mm, a width of 14.85 mm, and an inner (resp., outer) edge thickness of 1.286 mm (resp., 1.518 mm).

The cable samples were neither insulated nor vacuum-impregnated with resin. They were placed in 100-mm-long, stainless steel (316L) sample holders, made up of a U-shape base covered by a T-shape top. Two rows of four screws were located on each side of the top upper part. The screws could be tightened to predetermined torque values with a dynamometric wrench so as to apply a known perpendicular pressure to the cable broad face. The cable samples were cut at one end and were untwisted at the other end. Six of the untwisted strands were soldered to current leads and up to 15 strands were equipped with voltage taps. The taps were soldered as close as possible to the pressed length. The samples were prepared with great care to avoid any interstrand contact outside the sample holder. The samples and their holders were mounted, each at a time, on an insert. The insert was shoved into the bore of a superconducting dipole magnet and cooled down to 4.2 K.

The cable samples were heat treated in their sample holders prior to being mounted on the insert. The nominal heat treatment parameters were: up-ramp at 6 °C per hour to 660 °C, plateau at 660 °C for 240 hours, free down-ramp. ALS1 was heat treated at CEA/Saclay in Argon atmosphere, while ALS2 was heat treated at Alstom in a vacuum. The tops of the sample holders were put in place prior to heat treatment and were never removed. After heat treatment, it was determined that the screws of ALS1 were tightened to a torque corresponding to about 20 MPa on the cable while those of ALS2 were found to be more or less loose and were tightened to obtain 10 MPa.

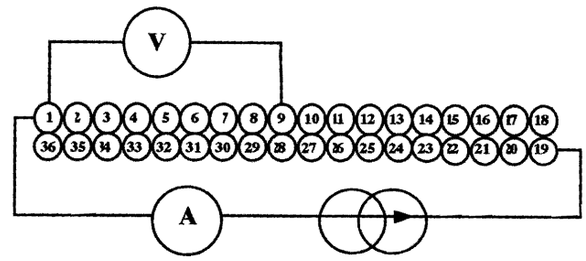

Fig. 2. Cable Sample Instrumentation.

IV. INTERSTRAND RESISTANCE MEASUREMENTS

The measurement procedure was as follows. The screws of the sample holders were tightened to a given torque. The insert was shoved into the vertical dewar and cooled down to 4.2 K. The background dipole magnet was ramped up to a given field. Two current leads were selected, and the voltage tap on the strand connected to the negative lead was chosen as potential reference (see Fig. 2). A current I was supplied to the leads, which was varied from 0 to I_{max} to 0 at a constant rate, and the voltages, V, between the instrumented strands and the reference were measured. The test was repeated for all available pairs of current leads. Once a series of measurements at a given field and a given pressure was completed, the background field was changed, or the insert was taken out, warmed up and the applied pressure was modified.

Fig. 3(a) presents a typical V=f(I) plot measured on ALS1 at 20 MPa and 0 T, while Fig. 3(b) presents a similar plot at 0.4 T. The data presented here correspond to a case where two diametrically opposite strands (strands 1 and 19 of Fig. 2) supply the current and V is the voltage across the two strands.

Let us first comment on Fig. 3(b). The voltage appears to vary linearly as a function of current, but there is a large hysteresis between the up- and down-ramps. It was verified that the amplitude of the hysteresis was proportional to the current ramp rate (which was kept constant throughout the test). Hence, it is likely that the hysteresis is due to inductive voltages picked up by instrumentation wires. If the ramp rate is constant, the inductive voltages are constant, and the slopes of the V = f(I) curves are not affected.

Let us now go back to Fig. 3(a). Once again, there is a large hysteresis between the up and down-ramps, but there also appears to be a break for a current, I_b, of about 172 A. For currents less than I_b, the curves are almost flat, while for currents greater than I_b, the curves vary linearly as a function of I, as observed in Fig. 3(b). When repeating the measurement in a small background field, B_a, the same phenomenon is observed, but the break takes place at a lower current. Plotting I_b as a function of B_a, shows that I_b decreases linearly and becomes nil for $B_a \approx 0.28$ T. For fields above 0.28 T, the voltage curves are similar to Fig. 3(b).

The break observed in Fig. 3(a) can be interpreted as follows. The Nb_3Sn strands manufactured by Alstom include seven sublelements surrounded by a tentalum inner barrier and

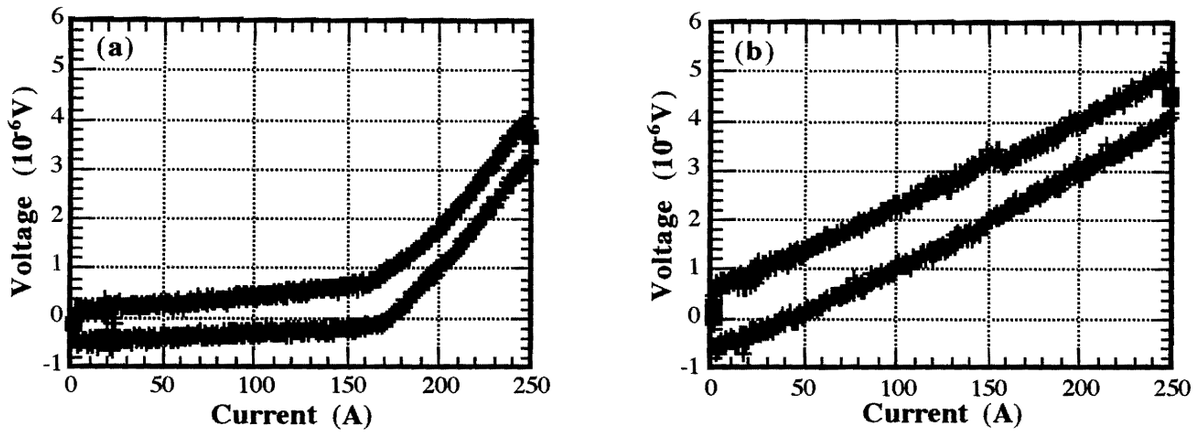

Fig. 3. Examples of $V = f(I)$ curves on ALS1: (a) at 20 MPa and 0 T and (b) at 20 MPa and 0.4 T.

a niobium outer barrier. It turns out that niobium is a type-II superconductor, with an upper critical field of 0.268 T at 4.2 K. When performing measurements in a background field lower than 0.268 T, the niobium barrier is initially in the superconducting state and transports all the current. Then, the interstrand resistances are mainly determined by the resistances of the copper sheath and of the surface oxide. However, as the supplied current is ramped up, the self-field effects increase and the critical current density of niobium decreases, until the barrier switches to the normal resistive state. Then, the current is redistributed towards the superconducting Nb_3Sn filaments inside the subelements and the interstrand resistances now encompass the resistances of the two barriers (plus that of a thin layer of bronze between the outermost filaments of the subelements and the inner barrier). Hence, the break seen in the curves of Fig. 3(a) is likely due to transitions of the niobum barriers. This hypothesis is confirmed by the fact that, when the background field is greater than the upper critical field of niobium, no breaks are observed.

In the following, we only consider data for a background field of 0.4 T (the largest one used during the tests). Furthermore, we determine the slopes of the $V = f(I)$ curves by fitting the up- and the down-branches by first order polynomials and by taking the average of the linear coefficients. These slopes have the dimension of resistances and are refferred to as *effective interstrand resistances*. They are characteristic of a given pair of current leads.

V. Interpretation of Interstrand Resistance Measurements

Let us consider a cable sample prepared and instrumented as described above and let i (resp., j) designate the strand number corresponding to the negative (resp., positive) current leads. Furthermore, let us assume that the crossover resistances dominate the sample interstrand resistances.

Over a pitch length, each strand crosses two times every other strand. The resistances of the two crossings are in parallel, and the overall crossover resistance per pitch length, r_c, is

$$r_c = \frac{R_c}{2} \tag{3}$$

Let k designate a strand number different from i and j. To go from strand i to strand j, the current has the choice between two types of parallel paths [14]: (1) a direct path through the r_c resistance connecting strand i to strand j or (2) indirect paths such as the one through the r_c resistance connecting strand i to strand k and that connecting strand k to strand j. When looking at the voltage, $(V_j - V_i)$, where V_i and V_j are the potentials of the taps connected to strands i and j, the direct path resistance is r_c, while that of an indirect path is $(2r_c)$. In an N-strand cable, there are $(N-2)$ such indirect parallel paths. It follows that $(V_j - V_i)$ can be estimated as

$$(V_j - V_i) \approx \frac{2r_c}{N} I \tag{4}$$

where I is the supplied current.

Furthermore, if r_c is uniform, the currents circulating in the $(N-2)$ indirect parallel paths are identical. Let I_k designate this common current value. We simply have

$$(V_j - V_i) \approx (2r_c)\, I_k \tag{5}$$

By combining (4) and (5), it follows that, for the chosen pair of current leads and for k, $k \neq i$ and $k \neq j$

$$(V_k - V_i) \approx r_c I_k \approx \frac{(V_j - V_i)}{2} \tag{6}$$

Equation (6) shows that, when plotting $(V_k - V_i)$ as a function of k, the voltage is constant, except for $k = i$, where it is nil, and for $k = j$, where it peaks at 2 times the constant.

Let us now consider the case of a cable sample where the interstrand resistances are dominated by the adjacent resistances and let us assume that $j > i$. Over a pitch length, each strand is connected to each of its neighbors by ($2N$) adjacent resistances in parallel. This corresponds to an overall adjacent resistance per pitch length, r_a, estimated as

$$r_a = \frac{R_a}{2N} \tag{7}$$

When supplying a current to strands i and j, the current has, in first approximation, the choice between two parallel paths [14]: (1) to go step by step, through the r_a resistances connecting strand i to strand (i+1), strand (i+1) to strand (i+2),... and strand (j-1) to strand j, or (2) to go step by step, the other way around, through the r_a resistances connecting strand i to strand (i-1),... strand 1 to strand N, strand N to strand (N-1),... and strand (j+1) to strand j. When looking at the voltage difference, ($V_j - V_i$), the first path corresponds to (j–i) resistances r_a in series, while the second path corresponds to (N–j+i) resistances r_a in series. It follows that, in this case, ($V_j - V_i$), can be estimated as

$$(V_j - V_i) \approx \frac{(j-i)(N-j+i)r_a}{N} I \tag{8}$$

Let I_1 (resp., I_2) designate the current in the first (resp., second) parallel path described above. We have

$$(V_j - V_i) \approx (j-i)r_a I_1 \approx (N-j+i)r_a I_2 \tag{9}$$

By combining (8) and (9), it follows that, when supplying current by strands i and j

$$(V_k - V_i) \approx \frac{(i-k)(j-i)r_a}{N} I \quad \text{for } k,\ 1 \le k \le i \tag{10a}$$

$$(V_k - V_i) \approx \frac{(k-i)(N-j+i)r_a}{N} I \quad \text{for } k,\ i \le k \le j \tag{10b}$$

and

$$(V_k - V_i) \approx \frac{(N-k+i)(j-i)r_a}{N} I \quad \text{for } k,\ j \le k \le N \tag{10c}$$

Equations (10) show that ($V_k - V_i$) increases linearly between $k = i$, where it is nil, and $k = j$, where it is maximum, and then decreases linearly from j to N and from 1 to i.

The potential distributions determined in the two extreme cases considered above are consistent with those derived from more sophisticated computations [12]. They are very different from each other and may offer a way of discriminating the prevailing type of interstrand resistances.

VI. DISCUSSION

Fig. 4 presents a plot of effective interstrand resistances as a function of strand number for two series of measurements performed on ALS1 and ALS2 at 100 MPa and for a 0.4 T background field. The two series correspond to a case where two diametrically opposite strands (strands 1 and 19 of Fig. 2) supply the current and the plotted data are normalized to the maximum effective interstrand resistance.

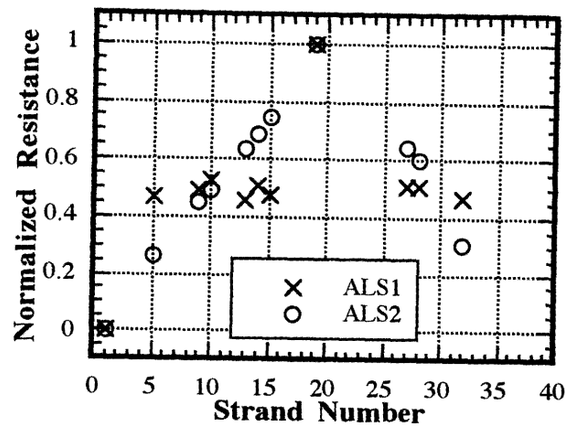

Fig. 4. Normalized effective resistance as a function of strand number for a regular and a cored Nb_3Sn cable at 100 MPa and 0.4 T

The data for ALS1 exhibit a more or less stable plateau with a peak corresponding to the strand connected to the positive lead. The average plateau value is 0.49. This behavior is consistent with that of a cable dominated by crossover resistances. The data for ALS2 increase linearly as a function of strand number between strands 1 and 19 and decrease, again more or less linearly, between strands 19 and 36. This behavior is consistent with what can be expected from a cored cable dominated by adjacent resistances.

Let us now try to estimate the actual values of R_a and R_c. For this, we developed a computer code, based on the equivalent electrical circuit of Fig. 1 applied to a cable pitch length. The code inputs are: number of cable strands, values of R_a and R_c, numbers of the strands connected to the current leads, and supplied current value. The main code routine computes the potentials at the network nodes, including those at the cable end where the voltage taps are located. Next, the code carries out an optimization and iteratively determines the values of R_a and R_c that minimize the root mean square of the difference between computed potentials and measured voltages.

In our experiments, the data analysis is complicated by the fact that the sample length, L_s = 100 mm, is somewhat longer than the cable pitch length, L_p = 73 mm. If L_s is equal to an integer number of times L_p, the total number of crossings between any two strands is ($2L_s/L_p$) and the total number of adjacent resistances between two neighboring strands is ($2NL_s/L_p$). It follows that the overall crossover and adjacent resistances per sample length, r_c^s and r_a^s, can be estimated as

$$r_c^s = \frac{R_c^*}{2} \quad \text{and} \quad r_a^s = \frac{R_a^*}{2N} \tag{11}$$

where

$$R_c^* = R_c \frac{L_p}{L_s} \quad \text{and} \quad R_a^* = R_a \frac{L_p}{L_s} \tag{12}$$

It seems reasonable to assume that (11) and (12) remain valid even when L_S is not equal to an integer number of times L_P. Then, we can use our measurement results and the computer code described previously to determine the optimum R_c^* and R_a^* and we can use (12) to estimate the actual values of R_c and R_a in our cable samples.

The optimization results for the measurements performed on ALS1 and ALS2 at 0.4 T are summarized in Table 1. ALS1 was tested at 5 successive pressures: 20 MPa, 10 MPa, 50 MPa, 100 MPa and 10 MPa, while ALS2 was tested at 4 successive pressures: 10 MPa, 50 MPa, 100 MPa and 10 MPa. For AlS1, we only retain the experimental data corresponding to current lead pairs where the normalized plateau value is between 0.4 and 0.6, while for ALS2, we only retain the data for which the variations as a function of strand number are more or less linear. The discarded profiles may be due to irregularities in the interstrand resistance distributions.

Table 1 shows that ALS1 is dominated by R_c. The R_c-values of ALS1 are about one order of magnitude smaller than R_a but are below the target of 20 $\mu\Omega$ set for LHC. Hence, this cable is probably not suited for accelerator magnets. Introducing a stainless steel core increases R_c by more than 2 orders of magnitude and ALS2 is dominated by R_a. The R_a-values of ALS2 are somewhat smaller than those of ALS1. Two reasons can explain this decrease: (1) the larger compaction of the cored cable, which may result in more strand deformations and larger contact surfaces and (2) the fact that ALS2 was heat treated in a vacuum where there is less risks of pollution or oxidation. The resistances of ALS1 show little evolution as a function of pressure, while those of ALS2 seem to increase slightly as a function of pressure and temperature cycles.

The Table 1 data can be compared to the interstrand resistances determined in [15] from calorimetric AC loss measurements on similar Nb_3Sn cables. Reference [15] uses an effective crossover resistance, $R_{c,eff}$, defined as

$$\frac{1}{R_{c,eff}} = \frac{1}{R_c} + \frac{20}{N^2 R_a} \qquad (13)$$

For ALS1 at 100 MPa: $R_{c,eff} \approx R_c \approx 1.1\ \mu\Omega$, and for ALS2: $R_{c,eff} \approx 80\ \mu\Omega$. These values are in good agreement with the ones quoted in [15]. However, Reference [15] concludes that the power dissipation of the cored cables remains dominated by crossover coupling currents. This is not the case for ALS2, where R_a is more than 100 times smaller than R_c, and thereby, P_a is larger than P_c. There is no obvious reason why the cables of [15] would behave differently.

VII. CONCLUSION

Two types of Rutherford-type cables with unplated Nb_3Sn strands were investigated: (1) a regular cable and (2) a cored cable. The regular cable is dominated by crossover resistances. These are very low and the cable is not suited for accelerator magnet applications. The cored cable satisfies the requirement on interstrand coupling currents, but it remains to be seen how it behaves in terms of interstrand current redistribution.

Table 1. Estimated values of crossover and adjacent resistances (in a 0.4 T background field).

Pressure (MPa)	ALS1 R_c ($\mu\Omega$)	ALS1 R_a ($\mu\Omega$)	ALS2 R_c ($\mu\Omega$)	ALS2 R_a ($\mu\Omega$)
10	1.4	5.6	150	1.5
50	1.1	20	180	1.8
100	1.1	11	275	1.7
10	1.1	11	240	1.9

REFERENCES

[1] K.-H. Mess, *et al.*, *Superconducting Particle Accelerator Magnet*, World Scientific, Singapore, p. 39 ff., 1996.

[2] A. Devred and T. Ogitsu, "Ramp-rate sensitivity of SSC dipole magnet prototypes," *Frontiers of Accelerator Technology*, World Scientific, Singapore, pp. 184–308, 1996.

[3] T. Ogitsu, *et al.*, "Influence of inter-strand coupling current on field quality of superconducting accelerator magnets," *Particle Accelerators*, **5 7**, pp. 215–235, 1997.

[4] M.N. Wilson and R. Wolf, "Calculation of minimum quench energies in Rutherford-type cables," *IEEE Trans. Appl. Supercond.*, **7** (2), pp. 950–953, 1997.

[5] A.K. Ghosh, *et al.*, "Minimum quench energies of Rutherford cables and single wires," *IEEE Trans. Appl. Supercond.*, **7** (2), pp. 954–957, 1997.

[6] J.M. Depond, *et al.*, "Examination of contacts between strands by electrical measurement and topographical analysis," *IEEE Trans. Appl. Supercond.*, **7** (2), pp. 793–796, 1997.

[7] J.D. Adam, *et al.*, "Rutherford cables with anisotropic transverse resistance," *IEEE Trans. Appl. Supercond.*, **7** (2), pp. 958–961, 1997.

[8] G.H. Morgan, "Eddy currents in flat metal-filled superconducting braids," *J. Appl. Phys.*, **4 4**, pp. 3319–3323, 1973.

[9] V.E. Sytnikov, *et al.*, "Coupling current losses in superconducting transposed conductors located in changing magnetic fields," *Cryogenics*, **2 9**, pp. 926–930, 1989.

[10] A.P. Verweij and H.H.J. ten Kate, "Coupling currents in Rutherford-type cables under time-varying conditions," *IEEE Trans. Appl. Supercond.*, **3** (1), pp. 146–149, 1997

[11] A.A. Akhmetov, *et al.*, "Periodicity of crossover currents in a Rutherford-type cable subjected to a time-dependant magnetic field," *J. Appl. Phys.*, **7 5**(6), pp. 3176–3183, 1994.

[12] D. Richter, *et al.*, "DC measurements of electrical contacts between strands in superconducting cables for the LHC magnets," *IEEE Trans. Appl. Supercond.*, **7** (2), pp. 786–792, 1997.

[13] C.E. Bruzek, *et al.*, "Development of superconducting wires for fusion application," *Advances in Cryogenic Engineering*, **4 2**(B), pp. 1369–1376, 1996.

[14] V.T. Kovachev, *et al.*, "Interstrand resistance of SSC magnets," *Cryogenics*, **3 4**(10), pp. 813–820, 1994.

[15] M.D. Sumption, *et al.*, "AC Loss and contact resistance in Nb_3Sn Rutherford cables with and without a stainless steel core," Presented at CEC/ICMC, Portland, OR, July 28–August 1, 1997.